

Voltage control in low voltage grids with independent operation of on-load tap changer and distributed photovoltaic inverters

*Original*

Voltage control in low voltage grids with independent operation of on-load tap changer and distributed photovoltaic inverters / Spertino, F.; Ciocia, A.; Mazza, A.; Nobile, M.; Russo, A.; Chicco, G.. - In: ELECTRIC POWER SYSTEMS RESEARCH. - ISSN 0378-7796. - 211:(2022), p. 108187. [10.1016/j.epsr.2022.108187]

*Availability:*

This version is available at: 11583/2969159 since: 2022-06-30T16:59:45Z

*Publisher:*

Elsevier Ltd

*Published*

DOI:10.1016/j.epsr.2022.108187

*Terms of use:*

This article is made available under terms and conditions as specified in the corresponding bibliographic description in the repository

*Publisher copyright*

Elsevier postprint/Author's Accepted Manuscript

© 2022. This manuscript version is made available under the CC-BY-NC-ND 4.0 license  
<http://creativecommons.org/licenses/by-nc-nd/4.0/>. The final authenticated version is available online at:  
<http://dx.doi.org/10.1016/j.epsr.2022.108187>

(Article begins on next page)



18 **Abstract:** This paper aims to find the optimal setups of voltage control devices in different  
19 configurations of Low Voltage (LV) grids with strong PhotoVoltaic (PV) diffusion by  
20 performing dedicated simulations. Distributed PV inverters and On-Load Tap Changer (OLTC)  
21 are simulated without considering their coordination, to avoid large investments in new  
22 communication infrastructures. Thus, each device independently works to decrease voltage  
23 deviations in the respective grid connection point. PV generation and consumption profiles are  
24 measured and used in two simulated LV grids, connected to the Medium Voltage (MV) grid by  
25 a MV/LV transformer with rated powers of 400 and 250 kVA, respectively. The calculation of  
26 the optimal devices setups is addressed as a multi-objective problem, considering objectives of  
27 voltage quality, grid losses, and OLTC lifespan increase. Multiple simulations are performed  
28 by varying the setup of the voltage controls, and considering different positioning and sizes of  
29 the generators. In the hardest case, the ratio between the maximum PV power generation and  
30 the maximum load in the whole grid is  $\approx 70\%$ . Pareto analysis is carried out to find the non-  
31 dominated solutions and TOPSIS is applied to rank the solutions. Finally, a sensitivity analysis  
32 is performed by changing the weights attributed to each objective function.

33

34 **Keywords:** Voltage control, low voltage grid, photovoltaic system, reactive power, on-load tap  
35 changer, Pareto front, sensitivity analysis, TOPSIS method.

36

## 37 **1. Introduction**

38 In the last decades, the increase of distributed generation in Low Voltage (LV) distribution grids  
39 lowered the energy production dependence from the centralized power plants. The number of  
40 distributed renewable energy systems, mainly PhotoVoltaic (PV) generators, is increasing,  
41 supporting the reduction of greenhouse gas emissions. Due to the fluctuations of solar  
42 irradiance, PV generation is highly variable and may lead to voltage fluctuations, reverse power

43 flows and power quality issues [1][2].

44 A general method to reduce voltage violations in LV grids calls for grid investments from the  
45 Medium Voltage (MV) connection point, e.g., with replacement of the MV/LV transformer  
46 and/or the reduction of the cable impedances [3]. However, these solutions are costly and only  
47 partially effective and hence, with larger and larger share of distributed generation (mainly PV  
48 systems), the LV grid operation will require more advanced voltage control techniques.

49 In the literature, many articles describe various methods to perform voltage control. It is clearly  
50 established that both centralized and local voltage controls have to be simultaneously present  
51 to ensure more options for effective voltage control. For centralized control, one of these  
52 methods involves the operation of the On-Load Tap Changer (OLTC), which modifies the tap  
53 position of the transformer to reach the voltage target. This device is mainly used on the High  
54 Voltage (HV) side of the HV/MV transformers, for controlling voltage in the MV grid.  
55 However, in recent years, it is also being used in LV grids [4]. For example, the unbalanced  
56 MV electrical grid (IEEE-123 nodes), characterized by a significant presence of PV generators,  
57 is analyzed in [5]. The control is carried out by OLTC and PV inverters that provide inductive  
58 or capacitive reactive power. In some cases, the voltage variation at the node with OLTC can  
59 cause voltage violations, especially in the nodes with high generation and low load. In this case,  
60 distributed control is fundamental because it acts locally at the node where the violation occurs  
61 [3]. It is noted that in [5] there is a communication system between inverters and the OLTC.  
62 With respect to [5], the MV grid analyzed in [6] is divided into several zones, each one equipped  
63 with an autotransformer and/or other devices, such as Capacitor Banks (CB), static reactive  
64 power compensators (STATCOM) and/or PV inverters. The logic for the reactive and active  
65 power control aims to minimize the number of tap changes of the OLTC by regulating more  
66 with other devices. Nevertheless, the study is based on the use of a communication system  
67 between the devices to perform real-time coordinate voltage control.

68 The IEEE 123-node MV grid is used in [7], with voltage control devices, such as Static Var  
69 Compensator (SVC) and OLTC, which communicate to improve voltages. The goal is to  
70 minimize different objective functions (total grid losses, number of tap changes, and SVC  
71 wear). To solve this multi-objective problem, a weight is assigned to each objective function.  
72 By changing the weights, the performance of each different control is discussed. In [8], the  
73 voltage is regulated by inverters that provide inductive or capacitive reactive power to stabilize  
74 the voltage at the Point of Common Coupling (PCC). They interact via a real-time  
75 communication system. Proportional Integral (PI) regulators are used to provide closed-loop  
76 voltage control between the grid and PV systems and make the control faster and more efficient.  
77 In [9], the voltage is regulated via PV inverters providing reactive power; PI regulators are used  
78 for the control logic, to decrease the voltage deviation and try keeping the losses low. In this  
79 case, centralized devices are not considered.

80 In [10], a mixed control is performed, with a coordination system among distributed and  
81 centralized devices. In particular, the grid is divided into several zones, each consisting of a  
82 certain number of cascaded devices. A ZIP-type load model is used, and the volt-var  
83 optimization method allows to reduce the number of tap changes. Three objective functions are  
84 defined, related to the number of tap changes, the Step Voltage Regulator (SVR) wear, and the  
85 generated active power. The first two objective functions are minimized, while the third one is  
86 maximized. From the results obtained, a decrease of the voltage deviation is due to the number  
87 of tap changes executed. Moreover, storage systems are used to improve the control  
88 performance. The MV grid in [11] is divided into zones, each of them is equipped with control  
89 devices (inverter, OLTC, CB and SVR). With respect to other papers, there is no  
90 communication system, every device is independent of others and regulates only the voltage in  
91 its PCC, and the distributed inverters use reactive power to control voltage.

92 Another method to control voltage in LV grids with high PV generation is the Active Power

93 Curtailment (APC) [12]. It consists of the reduction of active power generated to reduce the  
94 voltage at the PCC. In particular, there are two different approaches: in the first one, all inverters  
95 have the same reduction logic; in the second one, the setups are different. From the results  
96 obtained in [12], in the second approach a lower voltage deviation is obtained than in the first  
97 one, but with more Joule losses. The APC method is more efficient if there is a coordination  
98 between devices [13]. In the absence of a communication system, it is more convenient to  
99 regulate by providing only reactive power. In this way, the active power does not change, and  
100 the energy produced is maximized, as described in [14] and [15]. In these two works, the control  
101 is performed only by PV inverters that provide inductive or capacitive reactive power. The  
102 reactive and APC method can be combined, as in [12] and [16].

103 Furthermore, Battery Energy Storage Systems (BESS) can be used to increase the control  
104 effectiveness [16][17]. In [18] and [19], BESS and PV inverters are used to control voltage. In  
105 particular, in [20] each PV system is equipped with BESS which store energy only when the  
106 active power generated is greater than a threshold. This solution leads to a reduction of the  
107 voltage deviation. The work [19] studies how the control performance changes according to the  
108 characteristics of the grid. In urban grids characterized by relatively short distribution lines and  
109 non-negligible transformer parameters, with low R/X ratio (about 1), the reactive power  
110 provided by PV inverters is sufficient to adjust the voltage effectively. Instead, in rural grids  
111 characterized by longer distribution lines and higher R/X ratio (about 4÷5), it is advisable to  
112 regulate the voltage using PV inverters and BESS. The drawbacks of these last two works are  
113 the high cost of BESS and the absence of centralized devices. A solution that considers the costs  
114 in the optimization of LV distribution networks with OLTC, PV inverters and BESS is proposed  
115 in [20].

116 With respect to the analyzed papers, the present work does not consider coordination systems,  
117 and each device regulates the voltage independently and for each phase. Moreover, to maximize

118 the use of renewable sources, it is not considered the possibility to reduce the active power  
119 generated to mitigate the voltage issues. No BESS is included, to avoid the related costs. The  
120 present paper improves the work in [21], by describing in detail a more advanced procedure to  
121 perform the voltage control using centralized and distributed devices. In addition, Pareto  
122 analysis and TOPSIS are used to calculate the optimal setups of all the control devices. A  
123 sensitivity analysis is added to study the results variation as a function of the weights of the  
124 multi-objective problem. Finally, the whole procedure is applied to two different LV grids and  
125 results are discussed.

126 The next sections of this paper are organized as follows. Section 2 describes the voltage control  
127 methods. Section 3 describes the proposed procedure to find the optimal setups of the PV  
128 inverters and OLTC for the voltage control. Section 4 presents the case studies. Section 5 shows  
129 the simulation results. The last Section contains the conclusions.

130

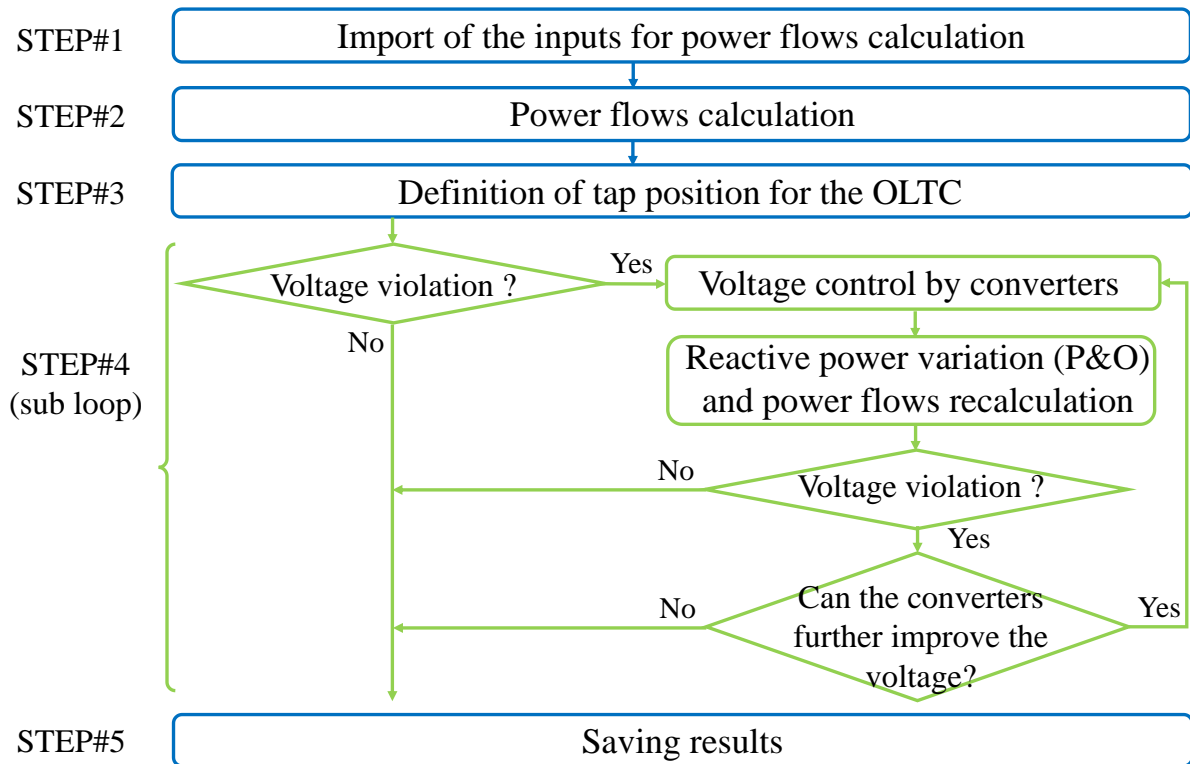
## 131 **2. Simulation of voltage control solutions**

132 The various aspects of simulating the voltage control by considering centralized and distributed  
133 Voltage Control Devices (VCDs) are addressed below. Section 2.1 describes the procedure used  
134 to simulate the operation of a LV grid with VCDs, i.e., an OLTC and distributed PV inverters.

135 After the general description of the whole procedure, Section 2.2 presents the details about the  
136 proposed logic for the voltage control performed by distributed PV inverters, that is, based on  
137 voltage criteria, voltage limits, and the logic to reach the optimal reactive power. Finally,  
138 Section 2.3 presents the logic used to perform voltage control by OLTC, showing the details of  
139 the procedure for the simulation of the OLTC operation and presenting a simple example of the  
140 effect of changing the setup parameters of the OLTC.

### 141 *2.1 Voltage control by centralized and distributed devices*

142 Fig. 1 shows the flowchart of the whole procedure to calculate the power flows and simulate  
 143 the voltage control for both centralized and distributed VCDs. Assuming steady state condition,  
 144 the procedure is repeated for each time step, which in the present work is 1 minute. The time  
 145 step of 1 min is typical for steady-state simulations for voltage control analysis [22][23][24]. It  
 146 permits to avoid the detailed modelling of dynamic processes of the equipment involved in the  
 147 voltage control. For example, in case of the OLTC equipped with transition resistors, the  
 148 transition between the resistors causes the current to vary during the switching process. In  
 149 particular, winding inductance, contact resistance and contact movement, interruptions and  
 150 arcing may affect the current amplitude [25][26]. The total operation time of an OLTC is  
 151 between few seconds to tens of seconds, depending on the respective design [27]. On these  
 152 bases, the time step of 1 min is sufficiently long to avoid the need of representing the dynamics  
 153 of the tap changers, which are faster.



154

155 Fig. 1. Procedure for power flows calculation and voltage control performed for each 1-min time step  
 156 of the simulation.

157 The procedure is composed of the following steps:



- 158 • STEP#1: the inputs for power flow calculation (e.g., grid data, generation and load  
159 profiles, capability curves, parameters of the controllers, voltage limits) are imported.  
160 From the second minute onwards, the inputs include the OLTC tap position, and the  
161 updated parameters of the OLTC proportional-integral control.
- 162 • STEP#2: a first power flow calculation is performed for time step  $t$  without change in the  
163 voltage control, with respect to the previous time step  $t-1$ . The Backward Forward Sweep  
164 (BFS) method is performed in the three-phase unbalanced LV grid. The equations to  
165 calculate the voltages and currents are indicated in [28]. The detailed procedure for power  
166 flow calculation and voltage control works according to [29].
- 167 • STEP#3: the tap position of the OLTC is calculated, according to the PI control described  
168 in Section 2.3.
- 169 • STEP#4: it consists of a sub-loop that can be run several times for each time step. A check  
170 of voltage violation for each node of the grid with a PV inverter is performed. In case of  
171 violation, the power flows are recalculated with the BFS by considering new reactive  
172 power quantities according to a logic which looks for the best quantity of reactive power  
173 to inject/absorb. The PV inverter continues to regulate, and simulations are repeated until  
174 there is no voltage violation, and not even one inverter can further improve the voltage  
175 (i.e., all control criteria are satisfied). The criteria that define if the inverters cannot further  
176 improve the voltage resulting in the exit from this sub-loop, and the logic to regulate  
177 reactive power, are described in Section 2.2.
- 178 • STEP#5: in absence of voltage violations or control possibility, the procedure exits from  
179 the loop, and data are saved.

180 The previously described procedure is repeated for each time step. At the end of the simulations,  
181 the losses and voltage indicators are calculated to compare the results obtained for different  
182 setups of the devices. All the calculations in this paper are performed by a Matlab<sup>®</sup> code written

183 by the authors.

## 184 2.2 Voltage control by distributed PV inverters

185 In case of voltage violations, the PV inverters provide inductive or capacitive reactive power to  
186 keep the voltage within the limits. In different countries, the standards require that the PV  
187 inverters can provide reactive power to support the grid operation. For example, the Italian  
188 standard CEI 0-21 used for LV grids [30] defines two capability curves depending on the rated  
189 active power  $P_{\text{rated}}$  of the PV system. The feasible operation region for the active and reactive  
190 power generated is located inside the corresponding capability curve. The numerical threshold  
191 on  $P_{\text{rated}}$  is determined by considering the rated voltage  $V_{\text{rated}} = 400$  V, the rated current  $I_{\text{rated}} =$   
192 16 A, and the power factor  $PF = 1$ , so that  $P_{\text{rated}} = \sqrt{3} V_{\text{rated}} I_{\text{rated}} PF_{\text{ref}} = 11.08$  kW. The  
193 formulation of the maximum power for the two capability curves is based on the reference  
194 power factor  $PF_{\text{ref}} = 0.9$ :

195 1) If  $P_{\text{rated}} \leq 11.08$  kW, the maximum reactive power depends on the active power  
196 generated  $P$ , as  $Q_{\text{max}}(P) = P \text{tg}(\arccos(PF_{\text{ref}}))$ , so that the power factor never decreases  
197 below the limit  $PF_{\text{ref}}$  [30].

198 2) If  $P_{\text{rated}} > 11.08$  kW, the maximum reactive power  $Q_{\text{max}}$  is constant and is determined as  
199  $Q_{\text{max}} = P_{\text{rated}} \text{tg}(\arccos(PF_{\text{ref}})) = 0.484 P_{\text{rated}}$ , independently of the active power generated.

200 In both cases, the capability curves are symmetrical with respect to the reactive power, so that  
201 the minimum reactive power is  $Q_{\text{min}}(P) = -Q_{\text{max}}(P)$  in the first case and  $Q_{\text{min}} = -Q_{\text{max}}$  in the  
202 second case.

203 As previously mentioned, in the present work there is no communication system, and each PV  
204 inverter manages reactive power independently of the others [31][32]. This logic is created to  
205 simplify the real implementation of Voltage Control Devices (VCDs) in actual grids. In fact,  
206 the whole procedure is based on the comparison between the voltage measured by the device

207 in its connection point and voltage limits. Each VCD does not require communication, because  
208 each device works autonomously, without cooperating with a centralized VCD (e.g., an OLTC)  
209 or other distributed VCDs. In a real implementation, the devices do not need to know advanced  
210 information about the grid, such as the number of nodes, the number of lines and the related  
211 impedances, etc. In fact, the VCDs operate only on the basis on the local information (the power  
212 flow is not calculated by VCDs). As a result, the VCDs logics do not change in case of the  
213 installation of additional distributed generation, or in case of changes in the grid configuration,  
214 which modify the impedance seen from the point of connection of the VCD.

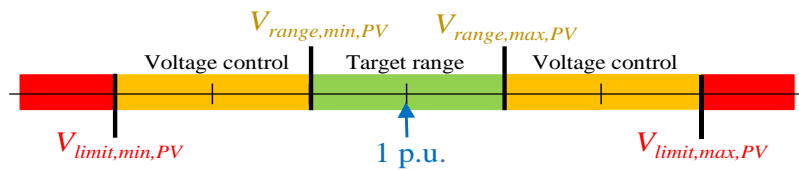
### 215 *2.2.1 Perturb & Observe technique for voltage control*

216 The control of one device can improve voltage in its node and can affect the other nodes. In this  
217 paper, the logic used to calculate the best reactive power quantity is based on the Perturb &  
218 Observe (P&O) technique. It is a logic widely used to obtain the maximum power point of the  
219 DC side of the PV inverters [33]. The principle of operation of the original P&O is briefly  
220 described with the following example. A PV inverter is working at a DC voltage power level  
221 defined by environmental conditions (irradiance and temperature). To reach the maximum  
222 output, the PV inverter increases the DC voltage of the PV modules and measures the new DC  
223 power production. If the production increases, the increase is repeated until there is no  
224 significant improvement of the power output. On the contrary, if the change in the DC voltage  
225 leads to a decrease of the output power, the procedure will be repeated in the opposite direction,  
226 i.e., by reducing the DC voltage [34]. In the present work, a similar P&O is used. The reactive  
227 power is changed to reduce the voltage deviation, i.e., the difference between the voltage  
228 measured at point of connection of the PV inverter with the grid and the reference voltage equal  
229 to 1 per unit (p.u.). In case of voltage violation, reactive power is added (capacitive for  
230 undervoltage, inductive for overvoltage): the electronic circuits in the PV inverter increase or  
231 decrease (with its sign) the phase angle between current and voltage to change the reactive

232 power injected or absorbed. If the voltage violation is reduced but not solved, the inverter  
 233 increases its reactive power. If the change in reactive power does not lead to a voltage  
 234 improvement, the control ends to avoid an unnecessary increase of the total Joule losses  $L_{tot}$ .

### 235 2.2.2 Voltage limits

236 The setup of the voltage control is changed by modifying the limits shown in Fig. 2 [29]:



237

238 Fig. 2. Voltage limits for the PV inverters contributing to voltage control

239 The inverters do not provide reactive power when the voltage is included in the range  
 240  $V_{range,min,PV} - V_{range,max,PV}$ . If the voltage is between  $V_{range,min,PV}$  and  $V_{limit,min,PV}$  or between  
 241  $V_{range,max,PV}$  and  $V_{limit,max,PV}$ , the inverter works to correct the voltage violation. In case of  
 242 overvoltage ( $V_i > V_{range,max,PV}$ ), the inverters provide inductive reactive power to reduce the  
 243 voltage. The proposed voltage control could work also in case of larger violations, i.e., the red  
 244 areas in Fig. 2 corresponding to a voltage lower than  $V_{limit,min,PV}$  or higher than  $V_{limit,max,PV}$ .  
 245 Nevertheless, in these cases, the voltage control is stopped to avoid interactions with other  
 246 logics included in the real applications. In fact, according to different grid codes [30][35], the  
 247 inverters have other tasks to perform: grid codes require the PV systems to provide low voltage  
 248 ride-through (LVRT) capability, i.e., the ability to withstand the abnormal voltage and remain  
 249 grid-connected in the event of grid failures [36]. The timing of LVRT is about hundreds of  
 250 milliseconds, very fast with respect to the time steps considered in this paper, and if the voltage  
 251 remains outside the limits for a longer period there is the disconnection of the PV inverter from  
 252 the grid, operated by the protection systems. As such, voltage control is active only inside the  
 253 voltage control ranges indicated in Fig. 2. A detailed discussion on LVRT capability is out of  
 254 scope for this paper.

### 255 2.2.3 Voltage control criteria

256 In the sub-loop described in the previous subparagraph, corresponding to STEP#4 in Fig. 1, at  
257 every iteration, each inverter has to respect a set of criteria to manage its reactive power. These  
258 criteria are used to guarantee the correct operation of the inverters and avoid useless reactive  
259 power in the grid. The individual inverters are not influenced by the criteria applied to the other  
260 devices and can be stopped in controlling voltage during an iteration, and restart in the next  
261 iteration. For example, let us suppose that, at the first iteration, an inverter in a generic node#A  
262 does not provide reactive power, because there is no violation in its PCC, but an increase in the  
263 reactive power injection in other nodes leads to a violation in node#A. Thus, the inverter in  
264 node#A will work to adjust its voltage until all its criteria are satisfied.

265 The criteria are:

- 266 • *Usefulness criterion*: if the voltage difference  $V_i^{(k)} - V_i^{(k-1)}$  between two iterations ( $k$  and  
267  $k-1$ ) is less than a threshold ( $V_i^{(k)} - V_i^{(k-1)} < \varepsilon$ ), the inverter stops the control to avoid a  
268 useless increase of the losses  $L_{tot}$ . A low value of  $\varepsilon$  makes the inverters to use all their  
269 reactive power. This threshold permits the inverters, that cannot significantly contribute  
270 to the improvement of voltage profiles, to exit from the loop.
- 271 • *Consistency criterion*: there is an inconsistency if the inverter provides inductive power  
272 and its PCC voltage increases, or if it provides capacitive power and the voltage  
273 decreases. The reason is that in these cases the control of the voltage is useless; voltage  
274 variation is dominated by other devices in the grid (for example another PV generator  
275 with a much higher power in a close node). In these cases, the inverter stops the reactive  
276 power variation.
- 277 • *Saturation criterion*: when the inverter exceeds the maximum reactive power according  
278 to its capability curve, it saturates and stops the control. Obviously, if a reactive power  
279 reduction is required, the inverter applies it.

### 280 2.3 Voltage control performed by OLTC

281 Centralized voltage control by On Load Tap Changer (OLTC) is based on PI control [29]. By  
282 changing the tap, the goal of the control is to keep the voltage at the LV side of the transformer  
283 as close as possible to the target voltage  $V_{\text{target}}$ . A key parameter of this control is the over-under  
284 voltage counter  $\alpha_{\text{OLTC}}(t)$ . The procedure to control the OLTC is shown in the flowchart in Fig.  
285 3:

- 286 • STEP# $\alpha$ : the data from the previous time step  $t-1$  are imported. They are the updated  
287 voltage counter  $\alpha_{\text{OLTC}}(t-1)$ , and the tap position to be used in time step  $t$ .
- 288 • STEP# $\beta$ : simulations are performed for time step  $t$ . From all the results (currents,  
289 voltages, power flows, losses, etc.), it is calculated the deviation  $\Delta V_{\text{OLTC}}$  between the  
290 simulated voltage at the LV side of the transformer  $V_{\text{OLTC}}$  and the target  $V_{\text{target}}$ .
- 291 • STEP# $\gamma$ : the voltage violation at the LV side of transformer is verified. In fact, to avoid  
292 excessive tap changes, the OLTC control changes if the voltage is outside or inside the  
293 deadband  $\pm DB$ .
- 294 • STEP# $\delta 1$ : in case of voltage violation (i.e.,  $|\Delta V_{\text{OLTC}}| > DB$ ) voltage counter  $\alpha_{\text{OLTC}}(t)$  is  
295 updated by adding or subtracting the quantity  $\alpha_{\text{OLTC},\Delta t}$ , as defined in (1):

$$296 \quad \alpha_{\text{OLTC}}(t) = \alpha_{\text{OLTC}}(t-1) \pm \alpha_{\text{OLTC},\Delta t}(t-1) \quad (1)$$

297 The increment  $\alpha_{\text{OLTC},\Delta t}$  is proportional to the absolute value of  $\Delta V_{\text{OLTC}}$ , as shown in (2):

$$298 \quad \alpha_{\text{OLTC},\Delta t}(t) = \frac{2 \cdot (|\Delta V_{\text{OLTC}}|)}{t_{\text{adm}} \cdot DB} \Delta t = \frac{2 \cdot (|V_{\text{OLTC}}(t) - V_{\text{bus,BT}}|)}{t_{\text{adm}} \cdot DB} \Delta t \quad (2)$$

299 where  $\alpha_{\text{OLTC},\Delta t}$  is inversely proportional to  $DB$  and depends on the admitted voltage  
300 violation time  $t_{\text{adm}}$  (whose effect will be shown in Fig.4). In the present work, the voltage  
301 deadband  $DB$  is equal to half a tap ( $DB = \Delta V_{\text{tap}}/2$ ). If the parameter  $\alpha_{\text{OLTC}}(t)$  exceeds the  
302 limits  $\pm 1$ , it is saturated at  $\pm 1$ .

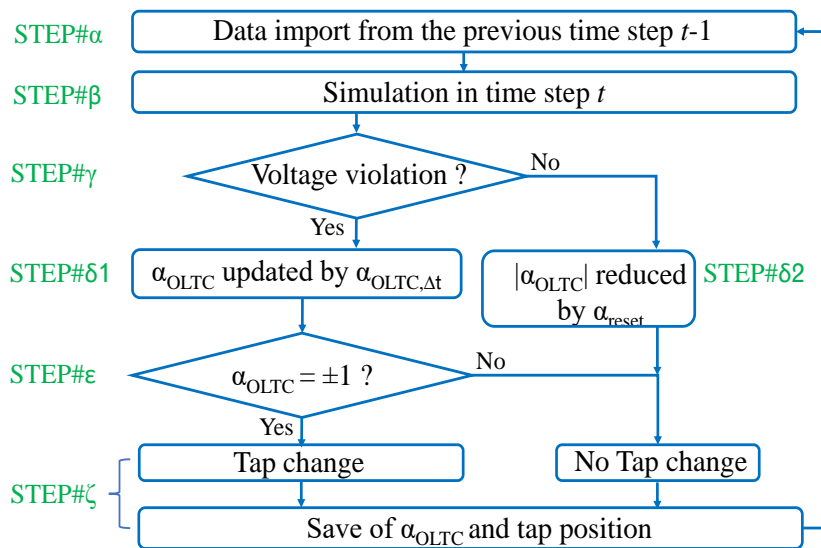
- 303 • STEP# $\delta 2$ : in case of no voltage violation ( $|\Delta V| < DB$ ),  $\alpha_{\text{OLTC}}(t)$  is partially reset. This  
304 partial reset is necessary to avoid unnecessary tap changes due to violations occurred

305 much earlier. For example, a temporary overvoltage occurred in the early morning should  
 306 not lead to a tap change in the late afternoon. Thus, at each step without voltage violation,  
 307 the parameter  $\alpha_{\text{reset}}$  (over-under voltage parameter) is used to decrease the value of  
 308  $\alpha_{\text{OLTC}}(t)$  according to (3):

$$309 \quad \alpha_{\text{OLTC}}(t) = \alpha_{\text{OLTC}}(t-1) \pm 1/\alpha_{\text{reset}} \quad (3)$$

310 The parameter  $\alpha_{\text{reset}}$  represents the time (in minutes) necessary to reset the counter  
 311  $\alpha_{\text{OLTC}}(t)$ . In fact, after a number of time steps with no violations equal to  $\Delta\alpha_{\text{OLTC}}$ , the  
 312 counter  $\alpha_{\text{OLTC}}(t)$  is restored back to zero.

- 313 • STEP# $\epsilon$ : if  $|\alpha_{\text{OLTC}}(t-1)|=1$ , the tap position changes at the beginning of the next time step  
 314  $t$ . If  $\alpha_{\text{OLTC}}(t)=1$ , the tap increases  $\text{tap}(t) = \text{tap}(t-1)+1$  for a lower voltage; if  $\alpha_{\text{OLTC}}(t)=-1$ ,  
 315 the tap decreases to obtain a higher voltage.
- 316 • STEP# $\zeta$ : in the last step, the updated value of  $\alpha_{\text{OLTC},\Delta t}$ , and the updated tap position to be  
 317 used in the next simulation, are saved. It is noteworthy that, after a tap change, a minimum  
 318 time  $t_{\text{min,two,taps}}$  is waited before permitting another one to avoid fast tap oscillations.

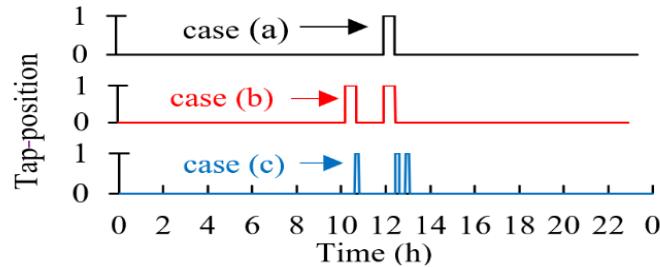


319  
 320 Fig. 3. Procedure for the control of the OLTC.

### 321 2.3.1 Example of the effect of the change of the setup parameters for the OLTC

322 As mentioned in STEP# $\delta 1$ , a key parameter to control the OLTC is the time  $t_{\text{adm}}$ ; it changes the

323 slew rate of the device limiting the number of tap changes  $N_{\text{tap}}$ . In fact, according to (2),  $\alpha_{\text{OLTC},\Delta t}$   
 324 and  $t_{\text{adm}}$  are inversely proportional. In conclusion, a high value of  $t_{\text{adm}}$  leads to a lower slew rate  
 325 of the OLTC. This is confirmed by the example presented in Fig. 4, in which three simulations  
 326 are presented. They are characterized by different parameters of proportional-integral control:  
 327 in case (a), the parameters are  $t_{\text{min,two,taps}}=30$  min,  $t_{\text{adm}}=20$  min,  $\alpha_{\text{reset}}=30$ . In case (b) the setup  
 328 is  $t_{\text{min,two,taps}}=30$  min,  $t_{\text{adm}}=5$  min and  $\alpha_{\text{reset}}=40$ ; in case (c) the setup is  $t_{\text{min,two,taps}}=10$  min,  
 329  $t_{\text{adm}}=5$  min and  $\alpha_{\text{reset}}=10$ . For the sake of clarity, only the first phase is represented in Fig. 4.  
 330 In case (a), during the whole day, the OLTC executes 2 tap changes, whereas in case (b) there  
 331 are 4 tap changes. In the last case, the number of tap changes is the highest (six) because all the  
 332 parameters are the lowest (have the lowest values). In cases (b) and (c), the OLTC is very  
 333 sensitive due to the low  $t_{\text{adm}}$ . The small value of  $t_{\text{min,two,taps}}$  in case (c) permits to perform more  
 334 tap changes in a reduced time frame.



335  
 336 Fig. 4. Tap position by varying  $t_{\text{min,two,taps}}$ ,  $t_{\text{adm}}$  and  $\alpha_{\text{reset}}$ .

337

### 338 3. Optimal Setups of Voltage Control Devices

339 The decision variables considered in this analysis are the parameters of the VCDs. The effects  
 340 of these parameters on the voltage profiles of the LV grids under study, as well as the Joule  
 341 losses in the lines and the number of tap changes of the OLTC, are taken into account and play  
 342 a fundamental role in the optimization process. Section 3.1 describes the indicator used to  
 343 evaluate the voltage deviations in the whole LV grid. Section 3.2 presents the complete lists of  
 344 the parameters used for setting up the VCDs; these are the inputs parameters that are changed



345 in each simulation scenario. The scenarios are created to study the effect of the change in the  
 346 inputs parameters on the optimization results. Finally, Section 3.3 presents the procedure to find  
 347 the optimal setups.

### 348 3.1 Voltage indicators

349 The calculation of voltage indicators allows to evaluate the effectiveness of each type of voltage  
 350 control. Among all the possible voltage indicators useful to calculate the quality of the voltage  
 351 profiles, the most important used in the present work is the Voltage Deviations with Energy  
 352 Flows (*VDEF*) [29]. It counts the sum of the squares of voltage deviations (with respect to a  
 353 reference value  $V_{ref}$ ) in each node  $k$  of the grid and at each time step  $t$ . Each deviation is  
 354 multiplied by the energy  $E_{k,t}$  to give more importance to the nodes and time steps in which the  
 355 consumption is higher [37]. This sum is divided by the total energy consumed in the grid during  
 356 the simulated period:

$$357 \quad VDEF = \frac{\sum_{t=1}^M \sum_{k=1}^{N_{nodes}} (V_{k,t} - V_{ref})^2 \cdot E_{k,t}}{\sum_{t=1}^M \sum_{k=1}^{N_{nodes}} E_{k,t}} \quad (4)$$

358 with  $M$  indicating the maximum number of time steps composing the timeframe  $T$ .

359

### 360 3.2 Input parameters of voltage control devices

361 According to [21], [29], [38], and this work, the variation of the input parameters (setup) of  
 362 distributed PV inverters affects the three objective functions  $L_{tot}$ ,  $N_{tap}$  and *VDEF* as follows:

- 363 •  $V_{limit,max,PV}$ : a reduction of this parameter leads to a restriction of the band delimited by  
 364  $V_{range,max,PV}$  and  $V_{limit,max,PV}$ , and the decrease of the *VDEF* of the grid. However,  $L_{tot}$   
 365 increases due to the inductive power supplied to reduce the overvoltage.
- 366 •  $V_{range,max,PV}$ : a reduction of this parameter leads to a restriction of the target range  
 367 delimited by  $V_{range,min,PV}$  and  $V_{range,max,PV}$ . In this case, the PV inverters provide more  
 368 inductive power to decrease the *VDEF* and to stabilize the voltage below the limit.

- 369 •  $V_{\text{range,min,PV}}$ : an increase of this parameter leads to a reduction of the target range between  
 370  $V_{\text{range,min,PV}}$  and  $V_{\text{range,max,PV}}$ . In this way,  $L_{\text{tot}}$  increases, but the  $VDEF$  decreases because  
 371 the inverters provide more capacitive power to stabilize the voltage above the limit.
- 372 •  $V_{\text{limit,min,PV}}$ : an increase of this limit leads to a reduction of  $VDEF$ , but  $L_{\text{tot}}$  can increase if  
 373 the inverters provide higher capacitive power to stabilize the voltage above the limit.

374 The effects of the variation of the setup parameters of the OLTC are described in the following  
 375 list:

- 376 •  $V_{\text{target}}$ : it is the voltage goal for the OLTC. The variation of this parameter leads to a  
 377 voltage variation in all the grid.
- 378 •  $t_{\text{adm}}$ : a reduction of this parameter leads to an increase of  $\alpha_{\text{OLTC},\Delta t}$ ; thus, the number of tap  
 379 changes  $N_{\text{tap}}$  increases leading to a reduction of  $VDEF$ .
- 380 •  $t_{\text{min,two,taps}}$ : an increase of this parameter leads to a reduction of  $N_{\text{tap}}$  because the tap  
 381 changer cannot work for a longer time after a step. Thus, the  $VDEF$  increases because of  
 382 a reduced operation of the OLTC.
- 383 •  $\alpha_{\text{reset}}$ : a high value of this parameter implies a lower slew rate of the OLTC; thus, a  
 384 reduction of the  $N_{\text{tap}}$  and an increase of  $VDEF$ .

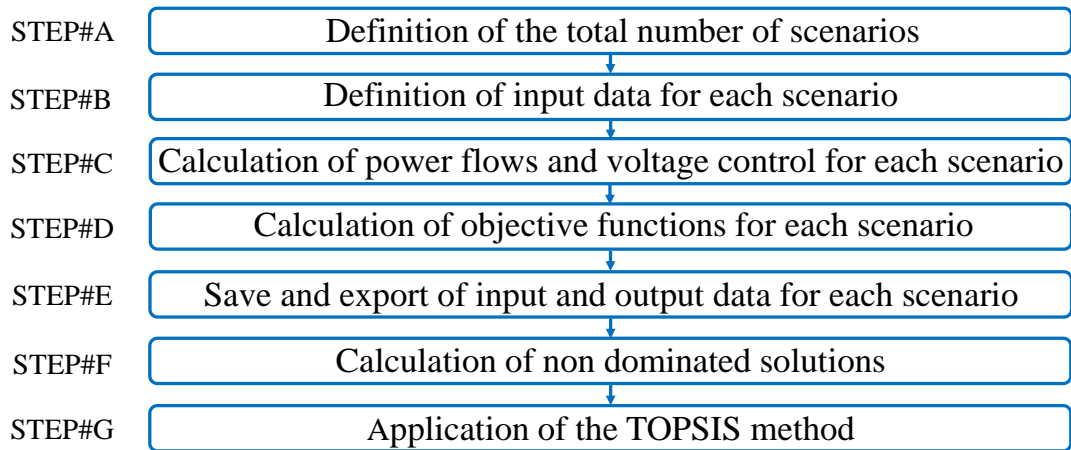
385 All the above parameters differ for every scenario and are randomly changed inside specific  
 386 ranges. For the voltage limits of inverters,  $V_{\text{limit,min,PV}} > 0.9$  and  $V_{\text{limit,max,PV}} < 1.1$ . According to  
 387 Fig. 2,  $V_{\text{range,max,PV}}$  and  $V_{\text{range,max,PV}}$  lie within those limits.

388 For the OLTC,  $V_{\text{target}}$  is close to unity,  $t_{\text{adm}}$  and  $t_{\text{min,two,taps}}$  are in the range 1÷30 min, and  $\alpha_{\text{reset}}$   
 389 varies between 1 and 30.

390

### 391 3.3 Calculation of the optimal setups for voltage control

392 Fig. 5 shows the proposed procedure to study and compare different setups of the voltage  
 393 control devices by solving the multi-objective problem.



394

395

Fig. 5. Procedure for the study of optimal setups of voltage control devices.

396

- STEP#A: the procedure starts with the selection of the total number of scenarios to be analyzed. It is an information that affects the simulation time.

397

398

- STEP#B: the inputs to be changed in each scenario are selected. They are the setup of the voltage control devices, e.g., the voltage limits of the capability curves of PV inverters and the parameters of the PI control. The complete list of the setup parameters was presented in the previous Section 3.2.

399

400

401

402

- STEP#C: the power flows are calculated, and the voltage control is performed. Each scenario has a different simulation performed according to the methodology explained in Section 2 for a timeframe  $T$  with time step  $t$ .

403

404

405

- STEP#D: the objective functions are calculated to perform the optimization. In the proposed procedure, the objective functions are the Joule losses for the whole grid  $L_{tot}$ , the number of tap changes  $N_{tap}$ , and the voltage indicator  $VDEF$ .

406

407

408

- STEP#E: all input and output data of each scenario are saved and organized for the next Pareto analysis.

409

410

- STEP#F: within all the sets of results, those that belong to the Pareto front are identified.

411

They represent the non-dominated solutions for which there is no objective function that

412

is simultaneously better for all the analyzed objective functions.

413 • STEP#G: the TOPSIS method [39] is applied to determine the ranking of the best  
414 solutions that belong to the Pareto front. It is noted that the results obtained with TOPSIS  
415 method depend on the weight assigned to each objective function. Moreover, the sum of  
416 all weights must be 1.

417

#### 418 **4. Case Studies and Grid Configurations**

419 The various aspects that refer to the preparation of the data for running the optimization  
420 procedure are described below. Section 4.1 contains the description of the two grids under  
421 analysis. Section 4.2 provides information about the measurement of generation and load  
422 profiles used as inputs for the simulations. Section 4.3 shows how the combination of the two  
423 grids and the measured profiles leads to the creation of different configurations. The resulting  
424 configurations correspond to the two grids considered, with renewable energy generators  
425 positioned in different nodes in the grid and with different nominal sizes.

##### 426 *4.1 Description of the case studies*

427 The simulations are performed on two LV grids:

- 428 1. Grid#1 (20 lines, 21 nodes); contains a three-phase transformer (20 kV/400 V, rated  
429 power  $S_{\text{rated,tr}} = 400$  kVA, rated current  $I_n = 570$  A, short-circuit impedance  $Z_{\text{SC}} = 24$  m $\Omega$   
430 and short circuit power losses at 75°C  $P_{\text{SC},75^\circ\text{C}} = 4.7$  kW).
- 431 2. Grid#2 (18 lines, 19 nodes); contains a three-phase transformer (20 kV/400 V, rated  
432 power  $S_{\text{rated,tr}} = 250$  kVA, rated current  $I_n = 361$  A, short-circuit impedance  $Z_{\text{SC}} \cong 38$  m $\Omega$   
433 and short circuit power losses at 75°C  $P_{\text{SC},75^\circ\text{C}} = 3.4$  kW).

434 In both grids, the slack node #0 is the MV bus of the MV/LV substation. In all the lines, the  
435 resistive component of the cables prevails over the inductive one. The LV grids have grounded  
436 neutral and lines with three-pole underground cables, except for the overhead cables in

437 proximity of the transformer. The structure of each grid is shown in [29]. The transformer is  
438 represented by the pi-model, neglecting the iron losses. The series impedance is calculated  
439 starting from the transformer datasheets. The tap changer has a voltage step of 1.25% of the  
440 nominal value and seven tap positions (-3,...,0,...,+3) corresponding to LV-side voltage  
441 changing in the range 0.9625 – 1.0375 p.u. when the transformer is supplied at nominal primary  
442 voltage.

#### 443 *4.2 Load and generation profiles*

444 Load and generation profiles have been measured using the Data Acquisition System (DAS)  
445 described in [40] and characterized by relative uncertainties equal to about 1%. The generation  
446 profiles consist of active power values measured during a week in September, which adequately  
447 represent an average generation along the year. These measured generation profiles are used as  
448 a reference sample: the generation in each node is recreated by amplifying the measured profiles  
449 without considering partial shading effects on the PV modules. On the contrary, the reactive  
450 power profiles from the PV inverters are simulated according to the voltage control described  
451 in the presented work. Regarding the load profiles, they are active and reactive power  
452 absorptions of the aggregation of apartments and offices.

#### 453 *4.3 Grid configurations*

454 In Grid#1, the ratio  $\theta_{PV}$  between the maximum power produced by all the PV generators and  
455 the maximum load in the whole grid is  $\theta_{PV,grid1} \approx 46\%$  due to an overall PV nominal power at  
456 AC side of 250 kVA. In Grid#2, this ratio is  $\theta_{PV,grid2} \approx 50\%$  due to an overall PV nominal power  
457 of 126 kVA. It is worth noting that the load and generation power peaks used to calculate these  
458 ratios are not simultaneous. For these two reference grid configurations, simulations are carried  
459 out by changing the position of load and generators or by increasing  $\theta_{PV}$ . The increase of  $\theta_{PV}$  is  
460 obtained selecting generation profiles with higher production. For each configuration listed in

461 Table 1, the procedure for the study of optimal setups (Fig. 5) is applied and results are  
 462 discussed in the next subparagraphs.

463 **Table 1. Grid Configurations**

Grid	Configuration	Description
1	CONF#1	Reference configuration for Grid#1
	CONF#2	Different positions of loads and generators
	CONF#3	Higher PV production peak - $\theta_{PV,grid1} \approx 55\%$
2	CONF#4	Reference configuration for Grid#2
	CONF#5	Different positions of loads and generators
	CONF#6	Higher PV production peak - $\theta_{PV,grid2} \approx 70\%$

464

## 465 5. Simulation Results

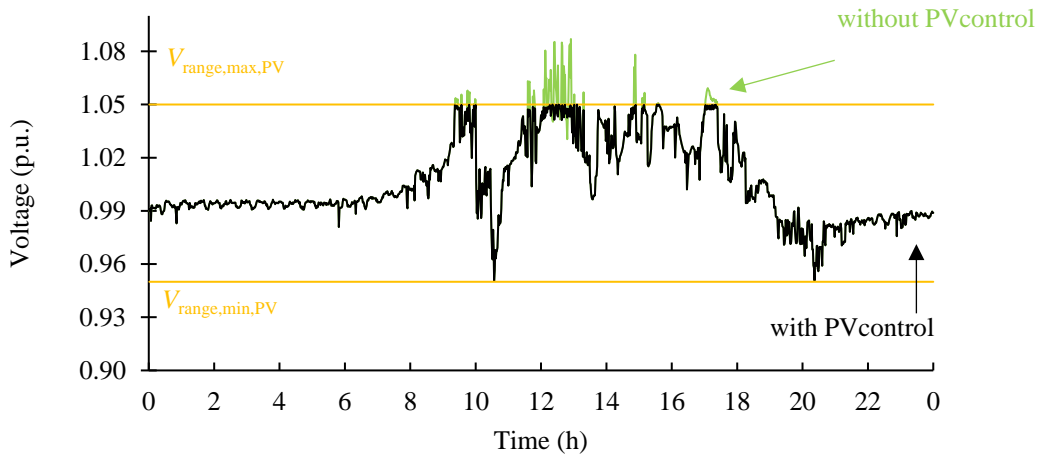
466 The results of the simulations performed are shown below. Section 5.1 presents examples of  
 467 daily voltage profiles obtained by controlling the PV inverters and the OLTC, following the  
 468 logics and procedures described in the previous sections. These examples are useful to better  
 469 understand the effects of the different voltage controls. For this purpose, the proposed graphs  
 470 show the controlled voltage profiles with respect to the same cases in which control is absent.  
 471 After the examples, Section 5.2 and Section 5.3 present the aggregated results of the simulation  
 472 of 6000 scenarios, each one with a different setup of the voltage controls. To compare the  
 473 results, a TOPSIS solutions ranking is applied, and the best scenarios are found from the  
 474 ranking. Finally, a sensitivity analysis is performed to analyze how the the ranking of the  
 475 solutions changes by using different weights for the objective functions.

476

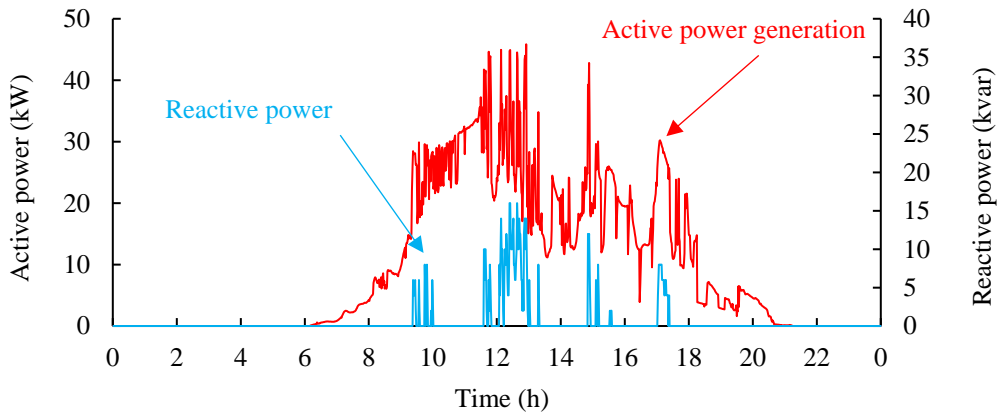
### 477 5.1 Examples of simulated voltage profiles obtained by controlling PV inverters and the OLTC

478 All types of voltage control are performed for a week with 1-minute time step. Fig. 6 shows a  
 479 daily example of voltage profiles calculated without voltage control (CONF#1, day#1, node  
 480 #18). In the figure, this profile can be compared with the one obtained in case of reactive power  
 481 control from the PV inverter. Profiles refer to node #18, that is, the one with the highest  
 482 impedance. The horizontal lines are the limits for the voltage control of the inverter. If the

483 voltage is higher than  $V_{range,max,PV}$ , the inverter provides inductive reactive power to stabilize the  
 484 voltage below the limit border. In this example, between hours 12:00 and 14:00, the voltage is  
 485 higher than the limit border due to the peak of PV production; thus, the inverter provides  
 486 inductive power (peak $\approx$ 15 kvar). No capacitive power is supplied because the voltage is never  
 487 below  $V_{range,min,PV}$ . The active and reactive power profiles related to Fig. 6 are shown in Fig. 7.  
 488 For the sake of clarity, all these profiles refer to the first phase of the unbalanced three phase  
 489 system.



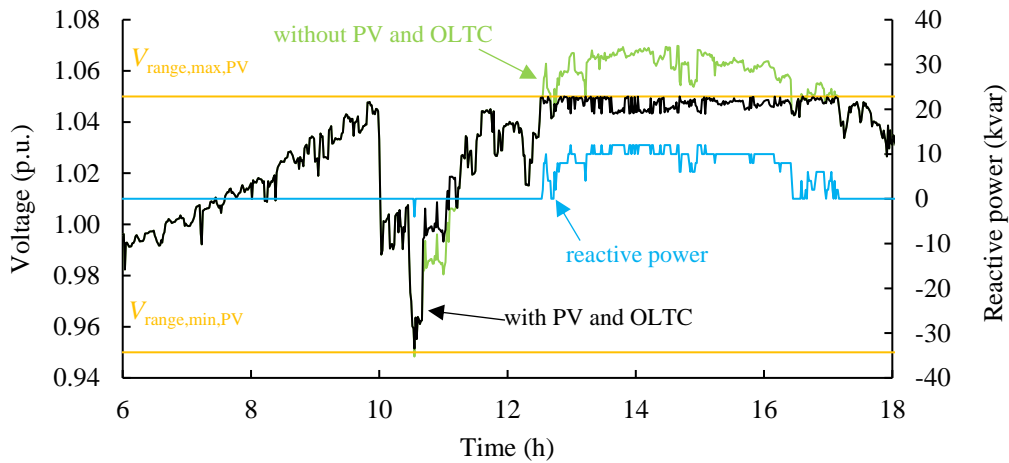
490  
 491 Fig. 6. Example of daily voltage profile: no control vs. reactive power from PV inverters - CONF#1,  
 492 day#1, node #18.



493  
 494 Fig. 7. Active and reactive profiles related to the example in Fig. 6.

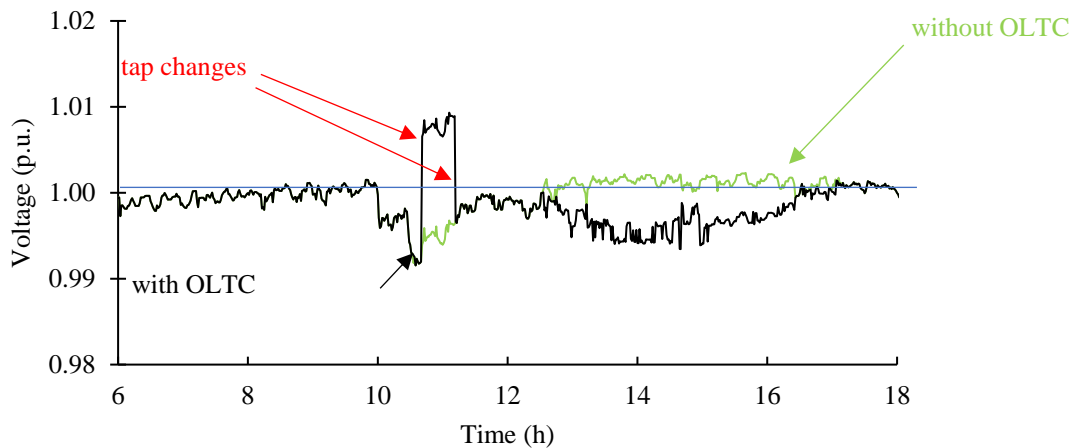
495 Fig. 8 shows another voltage profile calculated in case of voltage control performed from both  
 496 PV generators and the OLTC (Grid#1, day#2, node #18). At hour 10:30, the load increases  
 497 leading to an undervoltage; the PV power production is still too low, and inverters do not

498 contribute with capacitive power. The load increase influences the voltage at the PCC of the  
 499 OLTC (Fig. 9); it decreases the tap to adjust the voltage. After  $\approx 45$  min, the OLTC returns to  
 500 the previous position. After midday, the overvoltages are managed by the PV inverters, with no  
 501 other tap changes.



502  
 503  
 504

Fig. 8. Example of daily voltage profile: no control vs. OLTC+PV operation - CONF#1, day#2, node #18.



505

506  
 507

Fig. 9. OLTC operation related to the example in Fig. 8 - CONF#1, day#2, node #1 (LV side of the transformer).

508 Table 2 shows the values of the three objective functions  $VDEF$ ,  $L_{tot}$  and  $N_{tap}$  in case of voltage  
 509 control performed by PV inverters, with or without OLTC operation. All the results refer to the  
 510 whole week under analysis. In Grid#1, the  $VDEF$  decreases from  $2.99 \cdot 10^{-4}$  to  $2.90 \cdot 10^{-4}$  ( $\approx -5\%$ )  
 511 due to 8 tap changes. In Grid #2, the  $VDEF$  decreases from  $1 \cdot 10^{-4}$  to  $8.76 \cdot 10^{-5}$  due to 10 tap  
 512 changes ( $\approx -15\%$ ). In both examples, the OLTC operation does not interfere with inverters



513 leading to higher losses  $L_{tot}$  (in Grid#1 the increment is negligible).

514

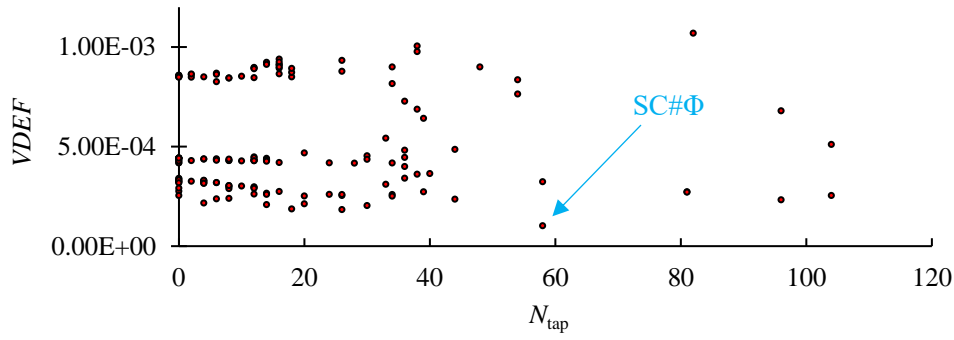
515

**Table 2. Losses and  $V_{def}$  with PV inverters or/and OLTC**

Grid	Objective function	Only PV inverters	PV inverters and OLTC
#1	$L_{tot}$ (kWh)	171	171
	$VDEF$	$2.99 \cdot 10^{-4}$	$2.90 \cdot 10^{-4}$
	$N_{tap}$ (phase 1)	-	8
#2	$L_{tot}$ (kWh)	54	54
	$VDEF$	$1 \cdot 05^{-4}$	$8.16 \cdot 10^{-5}$
	$N_{tap}$ (phase 1)	-	12

516 *5.2 TOPSIS solutions ranking*

517 The number of Scenarios (SC), simulated in the present work, is 1000 for each grid  
518 configuration, corresponding to a total of 6,000 scenarios. Each scenario starts with a different  
519 setup of the devices and includes a week of simulations with 1-min time step. For each grid  
520 configuration, the input parameters of voltage control devices are varied according to Section  
521 3.2. Fig. 10 shows the Pareto front related to the three objective functions obtained in CONF#1.  
522 For the sake of simplicity, this figure does not show the third objective function  $L_{tot}$ . In the  
523 Pareto front there is a Scenario (SC# $\Phi$ ) with minimum value of  $VDEF=1 \cdot 10^{-4}$ , while  $N_{tap} = 58$   
524 and  $L_{tot} = 674$  kWh are not the lowest. This particular case has very high losses with respect to  
525 the average  $\approx 150$  kWh. Thus, a 3D view is necessary to better understand the scenario  
526 distribution. Fig. 11 shows the 3D Pareto front. The SCs are divided in three groups in the front,  
527 identified by three rectangles. One group is characterized by scenarios with higher voltage  
528 deviations and lower losses. In the other two groups,  $VDEF$  is lower due to higher use of  
529 reactive power, leading to high  $L_{tot}$ . In every group, the number of tap changes is quite variable,  
530 but in most cases is lower than 50.



531

532

Fig. 10. Pareto front of two of the three objective functions – CONF#1.

533

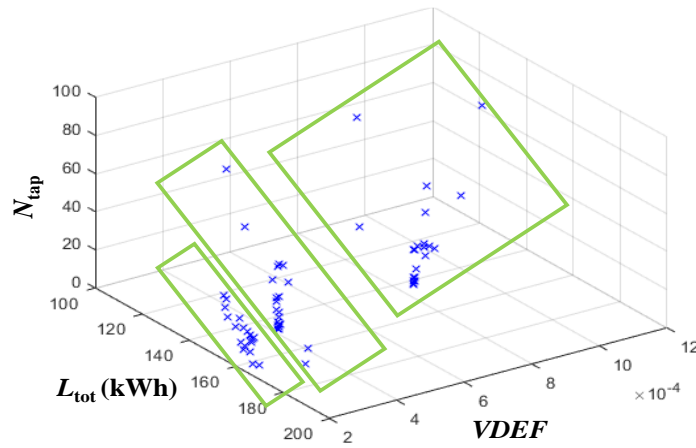
After the calculation of the 149 non-dominated solutions, the TOPSIS method is applied, and

534

the scenarios are ranked. In this case, the ranking weight for  $VDEF$  is  $w_{VDEF}=0.5$ , for the losses

535

$w_{L_{tot}}=0.4$ , and for the tap changes  $w_{N_{tap}}=0.1$ . Table 3 shows the resulting 5 best solutions.



536

537

Fig. 11. 3D Pareto front of the three objective functions – CONF#1.

538

**Table 3. Best Solutions with  $w_{VDEF}=0.5$ ,  $w_{L_{tot}}=0.4$  and  $w_{N_{tap}}=0.1$  - Configuration#1**

Ranking	BS#1	BS#2	BS#3	BS#4	BS#5
$VDEF (\cdot 10^{-4})$	2.16	2.37	2.40	2.53	2.61
$L_{tot}$ (kWh)	165	161	156	162	151.3
$N_{tap}$	4	6	8	0	12
$V_{limit,max,PV}$ (p.u.)	1.075	1.094	1.085	1.085	1.098
$V_{limit,min,PV}$ (p.u.)	0.920	0.909	0.923	0.905	0.919
$V_{range,max,PV}$ (p.u.)	1.072	1.092	1.075	1.056	1.065
$V_{range,min,PV}$ (p.u.)	0.986	0.982	0.981	0.975	0.972
$V_{target}$ (p.u.)	1.003	1.002	1.003	1.001	1.002
$t_{adm}$ (min)	29	14	19	30	13
$t_{min,two,taps}$ (min)	18	25	4	26	20
$\alpha_{reset}$	24	29	8	29	14

539

The Best Scenario BS#1 has minimum  $VDEF = 2.16 \cdot 10^{-4}$  and  $N_{tap} = 4$ . BS#2 has  $VDEF =$

540

$2.37 \cdot 10^{-4}$  and  $N_{tap} = 6$ . The other scenarios have similar results, with losses between 165 and

541 151 kWh. The main difference is in the number of tap changes; the OLTC responsivity is mainly  
542 influenced by  $t_{adm}$ . The key point is the setup of the inverters: the range  $V_{range,max,PV} - V_{limit,max,PV}$   
543 is small to limit the losses in the overvoltage management. Due to the reduced undervoltage in  
544 the case studies, the  $V_{limit,min,PV} - V_{range,min,PV}$  range is wide because it is less important for the  
545 loss increase. By changing the importance of losses, and focusing on voltage quality, the  
546 operation of inverter is boosted with a new set of weights, where  $w_{VDEF}$  is dominant,  $w_{VDEF}=0.8$ ,  
547  $w_{Ltot}=0.1$ , and  $w_{Ntap}=0.1$ ; the results are shown in Table 4. With this new set of weights, the  
548 range  $V_{range,max,PV} - V_{limit,max,PV}$  is always much higher than in Table 3. The OLTC operation  
549 increases the voltage quality, mainly due to low values of  $t_{adm}$ .

550 **Table 4. Best Solutions with  $w_{VDEF}=0.8$ ,  $w_{Ltot}=0.1$  and  $w_{Ntap}=0.1$ - Configuration#1**

Scenario Ranking	BS#1	BS#2	BS#3	BS#4	BS#5
$VDEF (\cdot 10^{-4})$	1.86	1.83	2.16	2.12	2.03
$L_{tot}$ (kWh)	234	227	165	188	190
$N_{tap}$	18	26	4	20	30
$V_{limit,max,PV}$ (p.u.)	1.082	1.080	1.075	1.077	1.071
$V_{limit,min,PV}$ (p.u.)	0.925	0.924	0.920	0.911	0.918
$V_{range,max,PV}$ (p.u.)	1.056	1.050	1.073	1.051	1.050
$V_{range,min,PV}$ (p.u.)	0.997	0.988	0.986	0.982	0.982
$V_{target}$ (p.u.)	0.998	1.003	1.003	1.002	1.004
$t_{adm}$ (min)	25	12	29	9	19
$t_{min,two,taps}$ (min)	30	27	18	3	15
$\alpha_{reset}$	16	21	24	3	3

551 *5.3 TOPSIS best solution in different grid configurations*

552 Table 5 shows the best solution obtained with TOPSIS for the different grid configurations.  
553 CONF#1 is not included in Table 5, because data are already BS#1 in Table 4. Again, the  
554 ranking weights are  $w_{VDEF}=0.8$ ,  $w_{Ltot}=0.1$  and  $w_{Ntap}=0.1$ .

555 **Table 5. TOPSIS Solution for Different Grid Configurations**

Configuration	#2	#3	#4	#5	#6
$VDEF (\cdot 10^{-4})$	2.00	2.23	5.32	4.52	1.01
$L_{tot}$ (kWh)	444.5	275.1	57.9	24.7	101.1
$N_{tap}$	18	16	6	8	2
$V_{limit,max,PV}$ (p.u.)	1.072	1.082	1.075	1.079	1.082
$V_{limit,min,PV}$ (p.u.)	0.920	0.925	0.920	0.924	0.925
$V_{range,max,PV}$ (p.u.)	1.021	1.056	1.073	1.058	1.095
$V_{range,min,PV}$ (p.u.)	0.966	0.997	0.986	0.917	0.914
$V_{target}$ (p.u.)	0.994	0.998	1.003	1.002	1.000

<b>Configuration</b>	<b>#2</b>	<b>#3</b>	<b>#4</b>	<b>#5</b>	<b>#6</b>
$t_{adm}$ (min)	20	25	29	6	21
$t_{min,two,taps}$ (min)	28	30	18	18	25
$\alpha_{reset}$	25	16	24	8	18

556

557 The best scenario in CONF#2 is particular, because the voltage target of the OLTC is generally  
558  $\approx 1$ . In this case, the target is lower leading to a high number of tap changes and high use of  
559 reactive power with the highest losses. Accepting a worsening, CONF#3 (despite the high PV  
560 injections) permits lower losses. In both cases, the setup of the OLTC is not the most responsive,  
561 and the number of tap changes is always below 20. In Grid #2 (CONF#4, #5 and #6) the same  
562 considerations can be applied.

#### 563 5.4 Sensitivity analysis of the TOPSIS weights

564 Another sensitivity analysis has been carried out to analyze how the results change by using  
565 different weights for the objective functions. Table 6 shows the results for the best scenario  
566 obtained for each set of weights in CONF#1. The sets of weights WS#3 and WS#6 lead to the  
567 same best scenario with the lowest  $VDEF$ , because  $w_{VDEF}$  is high. Thus, voltage control is the  
568 most efficient with many tap changes and high reactive power and losses. On the contrary,  
569 WS#4, WS#7 and WS#10 do not involve OLTC operation, with lower voltage quality. The  
570 other sets are compromises, where the best solution should be selected by the grid management.

571

**Table 6. Sensitivity Analysis of TOPSIS Weights - CONF#1**

<b>Weight Set</b>	<b><math>w_{VDEF}</math></b>	<b><math>w_{L_{tot}}</math></b>	<b><math>w_{N_{tap}}</math></b>	<b><math>VDEF (\cdot 10^{-4})</math></b>	<b><math>L_{tot}</math> (kWh)</b>	<b><math>N_{tap}</math></b>
1	0.5	0.4	0.1	2.16	165	4
2	0.4	0.4	0.2	2.16	165	4
3	0.8	0.1	0.1	1.86	234	18
4	0.2	0.4	0.4	2.76	152	0
5	0.3	0.6	0.1	2.40	156	8
6	0.9	0.05	0.05	1.86	234	18
7	0.3	0.2	0.5	2.53	162	0
8	0.7	0.2	0.1	2.16	165	4
9	0.1	0.1	0.8	2.53	162	0
10	0.3	0.1	0.6	2.53	162	0

## 572 6. Conclusions

573 The present study of voltage control in LV grids, performed by distributed PV inverters and  
574 OLTC, aimed to find the optimal setups for their operation without any coordination, even  
575 though a unique setup does not exist. Nevertheless, thanks to the result of the present work, the  
576 Distribution System Operators are given reference values to decide the setup for the distributed  
577 inverters to decide, considering their specific technical and economical constraints, how to face  
578 voltage issues. The Distribution System Operators can stress the control setups to improve  
579 voltage as much as possible, leading to higher Joule losses and maintenance cost, with less  
580 issues for the users. On the contrary, they can use less strict voltage control to avoid excessive  
581 increase in the costs.

582 The simulation results show how PV inverters can improve the voltage at their PCC adjusting  
583 their reactive power. Nevertheless, in LV grids the effects are limited, as the grid is not very  
584 inductive. On the contrary, the OLTC strongly affects the whole grid, but it cannot solve local  
585 voltage violations. Indeed, since there is no method of communication with other nodes of the  
586 grid, the OLTC may correct the voltage only at its PCC, where the voltage variation is low.  
587 Nevertheless, as shown in this work, implicit cooperation without communication between the  
588 OLTC and distributed PV inverters can be useful. The inverters will carry out a “*first*” partial  
589 voltage control. Simulations have shown that inserting large voltage ranges (i.e.,  $V_{\text{limit,min,PV}} -$   
590  $V_{\text{range,min,PV}}$  and  $V_{\text{range,max,PV}} - V_{\text{limit,max,PV}}$ ) involves an important increase in reactive power and  
591 losses to obtain a benefit on voltage. A large range with  $V_{\text{range,max,PV}} = 1.05$  and  $V_{\text{limit,max,PV}} \approx 1.08$   
592 generally leads to a large use of reactive power and many tap changes (an average of  $\approx 20$   
593 taps/day) to improve voltage with a resulting average value of  $VDEF \approx 2.14 \cdot 10^{-4}$ . Thus, for an  
594 optimal compromise between losses, voltage violations and lifespan increase of the OLTC, the  
595 ranges should be limited. Thus, the OLTC should solve the most serious voltage violations  
596 working as a “*second*” voltage controller. A lower range with  $V_{\text{range,max,PV}} = 1.07$  and  $V_{\text{limit,max,PV}}$

597  $\approx 1.08$  lead to a lower use of reactive power, and less tap changes (an average of  $\approx 7$  taps/day) to  
598 improve voltage; as a result the quality of voltage profiles is lower, with an average value of  
599  $VDEF \approx 1.83 \cdot 10^{-4}$ . With respect the previously mentioned larger range  $V_{\text{range,max,PV}} - V_{\text{limit,max,PV}}$ ,  
600 there is a drop in voltage quality of about 20%. The control by inverter and OLTC leads to  
601 better results when values of  $t_{\text{adm}}$  and  $t_{\text{min,two,taps}}$  are smaller. In this way, the control is more  
602 responsive to voltage variations. Therefore, the number of tap changes increases, and voltage  
603 deviation is reduced. For local voltage problems not solved by the studied control devices, the  
604 voltage quality could be improved by decreasing the impedance up to their PCC.  
605 Moreover, the present work has presented the procedure used to obtain the above-described  
606 results, in different setup scenarios and grid configurations. For each configuration, the Pareto  
607 analysis provides the non-dominated solutions. A TOPSIS analysis is included in the procedure  
608 to rank the scenarios. Finally, sensitivity analysis has been executed to evaluate how the results  
609 change according to the weights assigned to each objective function.

## 610 7. References

- 611 1. O.S. Nduka, L.P. Kunjumammed, B.C. Pal, A. Majumdar, Y. Yu, S. Maiti, A.R. Ahmad, Field Trial of  
612 Coordinated Control of PV and Energy Storage Units and Analysis of Power Quality Measurements, *IEEE*  
613 *Access*, vol. 8, pp. 1962–1974, 2020.
- 614 2. M. Pau, E. De Din, F. Ponci, P.A. Pegoraro, S. Sulis, C. Muscas, Impact of uncertainty sources on the voltage  
615 control of active distribution grids, *2021 International Conference on Smart Energy Systems and*  
616 *Technologies (SEST)*, pp. 1-6, 2021.
- 617 3. D. Zhang, J. Li, D. Hui, Coordinated Control for Voltage Control of Distribution Network Voltage Control  
618 by Distributed Energy Storage Systems, *Prot. and Contr. of Mod. Pow. Sys.*, vol. 3(1), pp. 1–8, 2018.
- 619 4. L. Del Rio Etayo, P. Cirujano, P. Lauzevis, G. Perez De Nalclares, A. Soto, A. Ulasenka, A new smart  
620 distribution transformer with OLTC for low carbon technologies integration, *24<sup>th</sup> Int. Conf. on Electricity*  
621 *Distribution*, paper no. 0832, Glasgow (UK), 12-15 June 2017.
- 622 5. A. Selim, M. Abdel-Akher, M.M. Aly, S. Kamel, T. Senjyu, Fast Quasi-static Time-series Analysis and  
623 Reactive Power Control of Unbalanced Distribution Systems, *International Transactions on Electrical*  
624 *Energy Systems*, vol. 29(1), ref. E2673, 2019.

- 625 6. M. Chamana, B.H. Chowdhury, F. Jahanbakhsh, Distributed Control of Voltage Regulating Devices in the  
626 Presence of High PV Penetration to Mitigate Ramp-Rate Issues, *IEEE Trans. on Smart Grid*, vol. 9(2), pp.  
627 1086–1095, 2018.
- 628 7. N. Daratha, B. Das, J. Sharma, Coordination Between OLTC and SVC for Voltage Control in Unbalanced  
629 Distribution System Distributed Generation, *IEEE Trans. on Power Systems*, vol. 29(1), pp. 289–299, 2014.
- 630 8. J. Ma, H. Ye, L. Haifeng, Z. Li, P. Han, Z. Lin, J. Shi, Research on Source-Network Coordination Voltage  
631 Control Strategy of Photovoltaic Power Plant Considering the Stability of Inverter Port Voltage, *E3S Web of  
632 Conferences*, vol. 143, ref. 2018, 2020.
- 633 9. E.M. Darwish, H.M. Hasanien, A. Atallah, S. El-Debeiky, Reactive Power Control of Three-phase Low  
634 Voltage System Based on Voltage to Increase PV Penetration Levels, *Ain Shams Engineering Journal*, vol.  
635 9(4), pp. 1831–1837, 2018.
- 636 10. V.B. Pamshetti, S.P. Singh, Optimal Coordination of PV Smart Inverter and Traditional Volt-VAR Control  
637 Devices for Energy Cost Savings and Voltage Control, *International Transactions on Electrical Energy  
638 Systems*, vol. 29(7), 2019.
- 639 11. M. Chamana and B.H. Chowdhury, Optimal Voltage Control of Distribution Networks With Cascaded  
640 Voltage Regulators in the Presence of High PV Penetration, *IEEE Trans. on Sustainable Energy*, vol. 9(3),  
641 pp. 1427–1436, 2018.
- 642 12. R. Tonkoski, L.A.C. Lopes, T.H.M. El-Fouly, Droop-based Active Power Curtailment for Overvoltage  
643 Prevention in Grid Connected PV Inverters, *2010 IEEE Int. Symp. on Industrial Electronics*, pp. 2388–2393,  
644 2010.
- 645 13. S. M. Rostami, M. Hamzeh, Reactive Power Management of PV Systems by Distributed Cooperative Control  
646 in Low Voltage Distribution Networks, *2021 29th Iranian Conference on Electrical Engineering (ICEE)*,  
647 2021, pp. 412-417.
- 648 14. A.M. Howlader, S. Sadoyama, L.R. Roose, S. Sepasi, Distributed voltage control using Volt-Var controls of  
649 a smart PV inverter in a smart grid: experimental study, *Renew. Energy*, vol. 127, pp. 145–157, 2018.
- 650 15. A.M. Howlader, S. Sadoyama, L.R. Roose, S. Sepasi, Distributed Voltage Control Method Using Volt-Var  
651 Control Curve of Photovoltaic Inverter for a Smart Power Grid System, *2017 IEEE 12th Int. Conf. on Power  
652 Electronics and Drive Systems (PEDS)*, pp. 630–634, 2017.
- 653 16. Z. Zhang, Y. Mishra, C. Dou, D. Yue, B. Zhang, Y.C. Tian, Steady-State Voltage Control With Reduced  
654 Photovoltaic Power Curtailment, *IEEE Journal of Photovoltaics*, vol. 10(6), pp. 1853–1863, 2020.
- 655 17. S. Wang, L. Du, X. Fan, Q. Huang, Deep Reinforcement Scheduling of Energy Storage Systems for Real-  
656 Time Voltage Regulation in Unbalanced LV Networks With High PV Penetration, *IEEE Trans. on  
657 Sustainable Energy*, vol. 12, no. 4, pp. 2342-2352, Oct. 2021.
- 658 18. F. Marra, G. Yang, C. Traeholt, J. Ostergaard, E. Larsen, A Decentralized Storage Strategy for Residential  
659 Feeders With Photovoltaics, *IEEE Trans. on Smart Grid*, vol. 5, pp. 974–981, 2014.
- 660 19. M.N. Kabir, Y. Mishra, G. Ledwich, Z.Y. Dong, K.P. Wong, Coordinated Control of Grid-Connected  
661 Photovoltaic Reactive Power and Battery Energy Storage Systems to Improve the Voltage Profile of a  
662 Residential Distribution Feeder, *IEEE Trans. on Industrial Informatics*, vol. 10(2), 967–977, 2014.

- 663 20. N. Efkarpidis, T. De Rybel, J. Driesen, Optimization control scheme utilizing small-scale distributed  
664 generators and OLTC distribution transformers, *Sustainable Energy, Grids and Networks*, vol. 8, pp. 74–84,  
665 2016.
- 666 21. A. Ciocia, G. Chicco, F. Spertino, Benefits of On-Load Tap Changers Coordinated Operation for Voltage  
667 Control in Low Voltage Grids with High Photovoltaic Penetration, *2020 International Conference on Smart  
668 Energy Systems and Technologies (SEST)*, 2020.
- 669 22. D.G. Infield, M. Thomson, Network power-flow analysis for a high penetration of distributed generation,  
670 *2006 IEEE PES General Meeting*, 2006.
- 671 23. J. Wang, X. Zhu, D. Lubkeman, N. Lu, N. Samaan, B. Werts, Load Aggregation Methods for Quasi-Static  
672 Power Flow Analysis on High PV Penetration Feeders, *2018 IEEE/PES Transmission and Distribution  
673 Conference and Exposition (T&D)*, pp. 1-5, 2018.
- 674 24. M. de Montigny et al., Multiagent Stochastic Simulation of Minute-to-Minute Grid Operations and Control  
675 to Integrate Wind Generation Under AC Power Flow Constraints, *IEEE Trans. on Sustainable Energy*, vol.  
676 4(3), pp. 619-629, 2013.
- 677 25. C. Plath, M. Putter, OMICRON electronics GmbH, Dynamic analysis and testing of On-Load Tap Changer  
678 with dynamic resistance measurement, Available online (accessed 31 March 2022):  
679 <https://www.omicronenergy.com/download/file/a207466e7bc405ecd22dbec942a41199/>
- 680 26. G.R. Chandra Mouli, P. Bauer, T. Wijekoon, A. Panosyan, E. Bärthlein, Design of a Power-Electronic-  
681 Assisted OLTC for Grid Voltage Regulation, *IEEE Trans. on Power Delivery*, vol. 30(3), pp. 1086-1095,  
682 2015.
- 683 27. D. Dohnal, On-load tap-changers for power transformers, Available online (accessed 31 March 2022):  
684 [https://www.reinhausen.com/fileadmin/downloadcenter/company/publikationen/f0126405\\_on-load\\_tap-  
685 changers\\_for\\_power\\_transformers.pdf](https://www.reinhausen.com/fileadmin/downloadcenter/company/publikationen/f0126405_on-load_tap-changers_for_power_transformers.pdf)
- 686 28. D. Shirmohammadi, H.W. Hong, A. Semlyen, G.X. Luo, A Compensation-based Power Flow Method for  
687 Weakly Meshed Distribution and Transmission Networks, *IEEE Trans. on Power Systems*, vol. 3(2), pp.  
688 753–762, 1988.
- 689 29. A. Ciocia, V.A. Boicea, G. Chicco, P. Di Leo, A. Mazza, E. Pons, F. Spertino, N. Hadj-Said, Voltage Control  
690 in Low-Voltage Grids Using Distributed Photovoltaic Converters and Centralized Devices, *IEEE Trans. on  
691 Industry Applications*, vol. 55(1), pp. 225–237, 2019.
- 692 30. Italian Electrotechnical Committee (CEI), Reference technical rules for the connection of active and passive  
693 users to the LV electrical Utilities, CEI Standard 0-21, December 2012 (In Italian).
- 694 31. A. Molina-Garcia, R.A. Mastromauro, T. Garcia-Sanchez, S. Pugliese, M. Liserre, S. Stasi, Reactive Power  
695 Flow Control for PV Inverters Voltage Support in LV Distribution Networks, *IEEE Trans. on Smart Grid*,  
696 vol. 8(1), pp. 447–456, 2017.
- 697 32. L. Collins, J.K. Ward, Real and Reactive Power Control of Distributed PV Inverters for Overvoltage  
698 Prevention and Increased Renewable Generation Hosting Capacity, *Renewable Energy*, vol. 81 pp. 464–471,  
699 2015.
- 700 33. A.F. Murtaza, M. Chiaberge, F. Spertino, U. T. Shami, D. Boero, M. De Giuseppe, MPPT technique based  
701 on improved evaluation of photovoltaic parameters for uniformly irradiated photovoltaic array, *Electric  
702 Power Systems Research*, vol. 145, pp. 248-263, 2017.



- 703 34. F. Spertino, J. Ahmad, A. Ciocia, P. Di Leo, A technique for tracking the global maximum power point of  
704 photovoltaic arrays under partial shading conditions, *2015 IEEE 6th International Symposium on Power  
705 Electronics for Distributed Generation Systems (PEDG)*, pp. 1-5, 2015.
- 706 35. D. Zeng, J. Guo, M. Ding, D. Geng, Fault ride-through capability enhancement by adaptive voltage support  
707 control for inverter interfaced distributed generation, *2015 5th International Conference on Electric Utility  
708 Deregulation and Restructuring and Power Technologies (DRPT)*, pp. 1924-1928, 2015.
- 709 36. D. Iioka, H. Saitoh, Enhancement of fault ride through capability using constant current control of  
710 photovoltaic inverters, *2016 IEEE Innovative Smart Grid Technologies - Asia (ISGT-Asia)*, pp. 1083-1088,  
711 2016.
- 712 37. E. Carpaneto, G. Chicco, M. De Donno, R. Napoli, Voltage controllability of distribution systems with local  
713 generation sources, *Bulk Power System Dynamics and Control*, Cortina d'Ampezzo, Italy, August 22-27,  
714 2004, pp. 261–273.
- 715 38. A. Ciocia, G. Chicco, P. Di Leo, M. Gai, A. Mazza, F. Spertino, N. Hadj-Said, Voltage control in low voltage  
716 grids: A comparison between the use of distributed photovoltaic converters or centralized devices, *Proc. 2017  
717 IEEE IEEEIC / I&CPS Europe*, pp. 1-6.
- 718 39. D.L. Olson, Comparison of weights in TOPSIS models, *Math. Comput. Model.*, vol. 40, no. 7-8, pp. 721–  
719 727, 2004.
- 720 40. F. Spertino, A. Ciocia, P. Di Leo, R. Tommasini, I. Berardone, M. Corrado, A. Infuso, M. Paggi, A Power  
721 and Energy Procedure in Operating Photovoltaic Systems to Quantify the Losses According to the Causes,  
722 *Solar Energy*, vol. 118, pp. 313–326, 2015.